Struct Chem (2015) 26:1389–1403
DOI 10.1007/s11224-015-0660-2

ORIGINAL RESEARCH

Opposite effect of Ca^{2+}/Mg^{2+} ions on the aggregation of native and precursor-derived $A\beta_{42}$

Ferenc Bogár[1] · Dóra Simon[2] · Zsolt Bozsó[2] · Tamás Janáky[2] · Szilvia Veszelka[3] · Andrea E. Tóth[3] · Mária A. Deli[3] · Attila Borics[4] · Zoltán Násztor[1,3] · Andrea Gyebrovszki[2] · Botond Penke[1,2] · Lívia Fülöp[2]

Received: 29 July 2015 / Accepted: 3 August 2015 / Published online: 12 September 2015

Abstract Work with the Alzheimer's disease-related synthetic peptide beta-amyloid (Aβ) is a challenging task because of its disadvantageous dissolution properties and high propensity for aggregation. Recently, a new synthetic derivative, iso-$A\beta_{42}$, has been introduced, which is a precursor of $A\beta_{42}$, and it offers advantages as concerns its synthesis and use for sample preparation. These two Aβ forms showed high similarity in their biological effects, as well as in their main structural characteristics under well-chosen experimental circumstances. When we changed these conditions, considerable dissimilarities appeared in the aggregation properties of the two peptides. In the present study, the aggregation pathways of native and precursor-derived $A\beta_{42}$ oligomers were compared in a physiological buffer with and without divalent metal ions (Ca^{2+}/Mg^{2+}). The presence of these ions influenced the Aβ conformations, the morphology as well as formation dynamics of aggregates in a different manner, as it was demonstrated by thioflavin-T-binding experiments, transmission electron microscopy and electronic circular dichroism measurements. Namely, the aggregation of native $A\beta_{42}$ to fibrils was facilitated, while the aggregation of precursor-derived $A\beta_{42}$ was hindered by these divalent metal ions. The observed differences in the aggregation had an impact also on the biological efficiency of native and precursor-derived $A\beta_{42}$ as it was elucidated by viability assays with enhanced sensitivity on primary endothelial cell cultures. Using replica exchange molecular dynamics, we modeled the conformational ensembles of the two investigated Aβ variants evolving during preparation process. We found considerable differences in the probability distribution of the conformers that can explain the observed dissimilarities in their aggregation properties.

Keywords Alzheimer's disease · Beta-amyloid aggregation · Divalent metal ions · Replica exchange molecular dynamics

Introduction

Research on Alzheimer's disease (AD) has recently undergone a pronounced paradigm shift in terms of the structure and toxicity relations of the beta-amyloid (Aβ) peptides involved in AD. The amyloid cascade hypothesis [1] had to be revised in its original form, as emerging evidences revealed that amyloid plaque burden does not necessarily correlate with the clinical progression of the disease [2]. The chase for the real pathogenic form of Aβ has resulted in the discovery of numerous specific aggregates of the peptide differing from mature fibrils, which are assumed to be the constituents of the extracellular plaques, but the toxicity of which cannot exclusively be held responsible for the pathophysiological processes involved in AD. The subfibrillar forms of the aggregates are

Dedicated to Prof. Magdolna Hargittai on the occasion of her 70th birthday.

✉ Lívia Fülöp
fulop.livia@med.u-szeged.hu

[1] MTA-SZTE Supramolecular and Nanostructured Materials Research Group of HAS, University of Szeged, Szeged 6720, Hungary

[2] Department of Medical Chemistry, University of Szeged, Dóm tér 8, Szeged 6720, Hungary

[3] Institute of Biophysics, Biological Research Centre of the Hungarian Academy of Sciences, Szeged 6726, Hungary

[4] Institute of Biochemistry, Biological Research Centre of the Hungarian Academy of Sciences, Szeged 6726, Hungary

classified according to size and shape, but the terms used in the literature are sometimes confusing. The fibrillar, but diffusible structures are the protofibrils [3], which can bind β-sheet-specific dyes, e.g., Congo red (CR) or thioflavin T (ThT), indicating that their conformations and neurotoxic effects are probably similar to those of their mature relatives. Non-fibrillar structures are termed Aβ oligomers. Although the process of oligomerization of amyloid precursor protein-derived Aβ monomers to fibrils is considered to be a dynamic equilibrium, oligomer forms possessing enhanced stability and lifetime have been isolated and identified by many groups. Small-n assemblies, such as dimers and trimers [4, 5], or dodecamers [6] isolated from biological sources, have been found to exert neurotoxic effects. Oligomers derived from synthetic Aβ have been prepared by standardized protocols and utilized successfully in biological experiments. Pioneering work in this field was the use of amyloid-derived diffusible ligands (ADDLs) [7], which can be prepared via a multistep dissolution protocol, involving the application of solubilizing agents such as 1,1,1,3,3,3-hexafluoro-2-propanol (HFIP) and dimethyl sulfoxide (DMSO) [8]. The oligomers are prepared in a mixture of DMSO and F12 medium, the oligomerization being facilitated by prolonged incubation at 4 °C. Many groups have applied this methodology successfully for the preparation of bioactive oligomers. Another widely accepted method for the oligomerization is to dissolve the peptide in NaOH solution, followed by dilution of the aggregate-free solution with physiological buffer [9]. Despite the great number of methods published so far, there has been no consensus on the size, structure and the most suitable preparation protocol of toxic $A\beta_{42}$ oligomers [10]. Recently, the molecular structure of Aβ fibrils originated from $A\beta_{40}$ and $A\beta_{42}$ oligomers was studied by NMR [11, 12] and scanning TEM [13] methods.

A new depsipeptide derivative, iso-$A\beta_{42}$ peptide, has been synthetized [14, 15] and utilized successfully as a precursor of native $A\beta_{42}$ for oligomer preparations [16]. Iso-$A\beta_{42}$ has advantageous structural properties in terms of solubility and propensity to aggregation relative to native $A\beta_{42}$. It possesses a bent structure in its original (post-synthetic) state, because of a depsipeptide bond between ^{25}Gly and ^{26}Ser. The transition into the native monomer structure, to meet the demands of the experimental setup, can be induced by a simple shift from acidic (2–3) to physiological neutral pH (7–7.4). Following an O → N acyl migration step, which takes place in seconds at physiological pH, the precursor peptide transforms into $A\beta_{42}$ and starts to aggregate, changing from an unordered, quasimonomeric structure to the biologically active, β-sheeted oligomeric form (Fig. 1).

The aggregation process of Aβ is highly sensitive to the physico-chemical environment, among others, like pH,

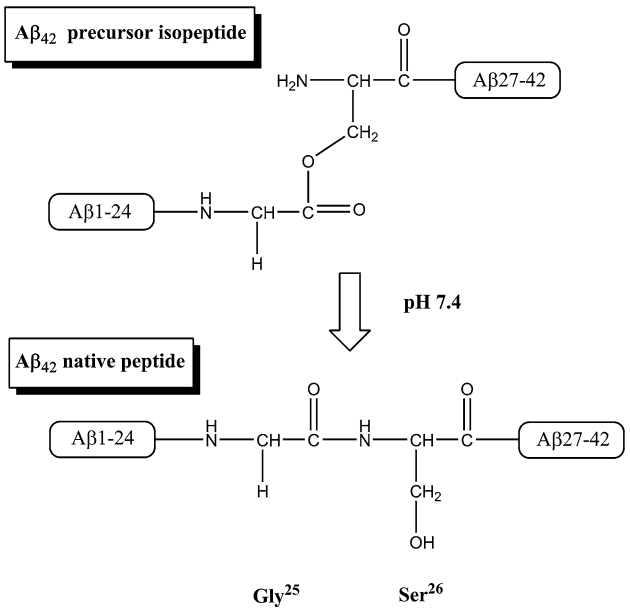

Fig. 1 Scheme of the iso-$A\beta_{42}$ → native $A\beta_{42}$ conversion

solvent, or the presence, quality, and concentration of ions in the solution [17]. This phenomenon is also related to the Hofmeister effect at elevated concentrations, and depends on the kosmotropic-chaotropic character of the coexisting ions. On the other hand, it was also demonstrated that calcium ions are able to accelerate the $A\beta_{42}$ aggregation already at physiological concentrations [18, 19] where the Hofmeister effect is negligible. Recently Brannstrom et al. [20] revealed the dynamic, reversible character of this ionic influence as well.

In another study, the central fragment of Aβ was investigated in a molecular dynamics simulation to elucidate the influence of Na, K, Ca, and Mg ions on the structure of Aβ(21–30) [21]. It was pointed out that the presence of Ca^{2+} (and in a smaller extent also Mg^{2+}) ions increased the random coil structure propensities by diminishing intramolecular hydrogen bonds.

The aim of the present work is the characterization of the aggregation properties of native $A\beta_{42}$ and the precursor iso-$A\beta_{42}$-derived assemblies and the toxicity of the oligomers. The effects of divalent metal ions present in the buffer on the aggregation pathway are examined with the aid of ThT-binding, transmission electron microscopy (TEM), and electronic circular dichroism (ECD) spectroscopy. It is also demonstrated by biological experiments that Ca^{2+} and Mg^{2+} play important roles in the control of in vitro aggregation, which can influence conformational stability and the biological activity (toxicity) of samples prepared from synthetic $A\beta_{42}$. For this purpose, we compare the cytotoxic effects of amyloid aggregates formed with or without Ca^{2+} and Mg^{2+} on primary rat brain

endothelial cells, which are very sensitive to $A\beta_{42}$ [22, 23]. Eventually, we attempt to explain the different behavior of the two investigated Aβ forms upon aggregation in the presence of Ca^{2+}/Mg^{2+} by the conformational differences of their monomers. We point out that the conformational ensembles of the two Aβ forms evolving during the preparation phase show characteristic differences that can explain dissimilarities in their aggregation pathways.

Materials and methods

In this manuscript, we refer to the unmodified synthetic $A\beta_{42}$ sequence as 'native $A\beta_{42}$,' to the synthetic precursor form with the depsipeptide bond as 'iso-$A\beta_{42}$,' and to the form which is derived from the precursor iso-$A\beta_{42}$ by pH switch as 'precursor-derived $A\beta_{42}$.'

Ethics statement

No procedures involving experiments on human subjects were done in this study. Animal care followed the recommendations of European Convention for the Protection of Vertebrate Animals Used for Experimental and other Scientific Purposes (Council Directive 86/609/EEC) and the NIH Guide for Care and Use of Laboratory Animals (NIH publications no. 80-23). Formal approvals to conduct all animal procedures in the experiments have been obtained from the local authority, Csongrád County Animal Health and Food Control Station (permit number: XVI./834/2012).

Chemicals used in the experiments

All materials, solvents, buffer salts, and reagents for the determination of the peptide content were purchased from Sigma-Aldrich, Budapest, Hungary; Fmoc- and Boc-protected amino acids, *N*,*N*′-dicyclohexylcarbodiimide (DCC), *N*,*N*′-diisopropylcarbodiimide (DIC), 1-hydroxy-7-azabenzotriazole (HOAt), and 1-hydroxybenzotriazole (HOBt) from GL Biochem Shanghai, China; and Fmoc-Ala-Wang and Boc-Ala-PAM resins from Bachem, Bubendorf, Switzerland.

Native $A\beta_{42}$ and iso-$A\beta_{42}$ were synthetized in-house, as reported elsewhere [16, 24]. Briefly, both peptides were synthetized manually following standard solid-phase peptide synthesis protocols: native $A\beta_{42}$ with Fmoc chemistry using DCC/HOBt activation on Fmoc-Ala-Wang resin, and iso-$A\beta_{42}$ with Boc chemistry using DIC/HOAt activation on Boc-Ala-PAM resin. The crude peptides were purified by high-performance liquid chromatography (HPLC). Fractions were pooled according to their purity, checked by analytical HPLC and electrospray ionization mass spectrometry. Amino acid analysis indicated a peptide content of 76.5 % (by weight) for the non-aggregated native $A\beta_{42}$ and 73.2 % for iso-$A\beta_{42}$. These data were used upon sample preparation with corrections for the required peptide amounts.

Sample preparation protocols

Samples for ThT measurements

Native $A\beta_{42}$ and iso-$A\beta_{42}$ were incubated in HFIP overnight in order to remove preformed aggregates. Solution aliquots were then transferred to Eppendorf tubes, and HFIP was removed *in vacuo*. The resulting peptide film was stored at −20 °C and used within 1 month. Prior to use, the peptides were dissolved in one of the following physiological buffers: (a) $NaHCO_3$-buffered saline (HCBS: 20 mM $NaHCO_3$ 154 mM NaCl, saturated with CO_2) or (b) HCBS supplemented with $CaCl_2$ and $MgCl_2$ (20 mM $NaHCO_3$ 154 mM NaCl, 2.3 mM $CaCl_2$, 1 mM $MgCl_2$ saturated with CO_2).

Samples for ECD and transmission electron microscopy (TEM) measurements and biological studies

Peptide stocks were prepared identically as for ThT measurements. The solutions were diluted in HCBS buffer at pH 7.4, with or without Ca^{2+} and Mg^{2+}, to the following nominal concentrations: ECD measurements: 12.5 μM, and TEM measurements and biological studies: 75 μM. In the latter case, both native $A\beta_{42}$ and precursor-derived $A\beta_{42}$ were tested freshly prepared and after incubation at 37 °C for 24 h. Peptide stocks were diluted to 50 μM with cell-culturing medium prior to cell treatment.

ThT measurements

ThT was dissolved in 50 mM NaH_2PO_4/Na_2HPO_4 buffer (pH 7.0) to give a final concentration of 25 μM. This working solution was kept at 4 °C protected from light and used for at most 1 week. Samples were incubated for 1 week; aliquots were removed for ThT measurements at 0 min, 1, 3, 6, 24, 48, and 168 h. At each time point, aliquots from the incubated peptide solutions were mixed with the working solution in a ratio which resulted in a uniform peptide concentration (4 μM). Mixtures were vortexed and 150 μL aliquots were placed on a 96-well plate. ThT fluorescence was measured on a plate reader at $\lambda_{ex} = 450$ nm and $\lambda_{em} = 480$ nm. Mean values and SD were calculated from the results of three parallel measurements.

TEM

A 10 μL oligomer solution was placed on a formvar-carbon-coated 400-mesh copper grid (Electron Microscopy Sciences, Washington, PA, USA) and stained with uranyl acetate. The aggregates were characterized by TEM on a Philips CM 10 transmission electron microscope (FEI Company, Hillsboro, OR, USA), operating at 100 kV. Images were taken with a Megaview II Soft Imaging System, routinely at magnifications of ×46,000 and ×64,000, and analyzed with an AnalySis® 3.2 software package (Soft Imaging System GmbH, Münster, Germany).

ECD spectroscopy

ECD spectra of the peptides were recorded on a Jasco (Tokyo, Japan) J815 spectropolarimeter equipped with a Peltier temperature controller using either a 1-mm- or a 2-mm-path-length quartz cell. Spectra of peptide solutions in the wavelength region 200–250 nm were recorded at 37 °C and 100 nm/s scan speed. The reported spectra are accumulations of 10 scans, from which the similarly recorded, corresponding solvent spectra were subtracted.

Molecular dynamics simulation

REMD [25, 26] simulation was used to identify structural differences between native $A\beta_{42}$ and iso-$A\beta_{42}$ monomers formed during the HFIP treatment which is part of the sample preparation protocol. HFIP is known to induce intra- rather than intermolecular interactions in peptides, suppressing aggregation. For practical purposes, HFIP was substituted in the simulations with trifluoroethanol (TFE), which has the same effect on peptide structure. As Aβ peptides were prepared in an acidic environment (pH 2), the titratable residues were protonated accordingly.

Simulation was started with a 2000-step minimization, followed by 5 ns constant pressure dynamics at 300 K for equilibration of the system. In the REMD simulation, 48 temperatures were chosen between 300 and 410 K. Each replica was heated up to the simulation temperature during 10 ns. Starting from this, 100-ns production Langevin dynamics simulations were performed at each temperature. Exchange between neighboring replicas was attempted every 2 ps, resulting in a final exchange rate between 0.15 and 0.2.

AMBER ff98SB force field parameters [27] were assigned to the peptides, and REMD calculations were performed using the Gromacs 4.5 package [28]. The missing parameters of the protonated and modified residues in the iso-$A\beta_{42}$ and of the TFE solvent were supplied from the generalized amber force field (GAFF) [29]. The restrained electrostatic potential (RESP) method [30] was applied to calculate the charges of these constituents.

The last 50 ns of the lowest-temperature (300-K) replica were selected to characterize the conformational assemblies of both native $A\beta_{42}$ and iso-$A\beta_{42}$ monomers. Secondary structure analysis was performed with the aid of the recently published dihedral-based segment identification and classification (DISICL) method [31]. The H-bonded network was investigated with the VMD program, which was also used for figure preparations. Compactness of the Aβ conformers were characterized with their radius of gyration as it is calculated by the g_gyrate utility of Gromacs 4.5. Although the applied method and simulation time may not be sufficient to describe the complete folding process, they facilitate identification of the local structural elements that fundamentally influence the final structures.

Cell culture

Primary cultures of rat cerebral endothelial cells were prepared from 2-week-old rats, as detailed earlier [22, 32]. Forebrains were collected in ice-cold sterile PBS; meninges were removed, and gray matter was minced with scalpels to 1 mm^3 pieces and digested with 1 mg/mL collagenase CLS2 (Worthington, Lakewood, NJ USA) in Dulbecco's modified Eagle medium (DMEM) for 1.5 h at 37 °C. Microvessels were separated from myelin-containing elements by centrifugation in 20 % bovine serum albumin (BSA)–DMEM (1000×*g*, 20 min), and further digested with 1 mg/mL collagenase–dispase (Roche Hungary, Budaörs, Hungary) in DMEM for 1 h. Microvascular endothelial cell clusters were separated on a 33 % continuous Percoll gradient (1000×*g*, 10 min), collected, and washed twice in DMEM before plating on collagen type IV and fibronectin-coated dishes (Falcon, Becton–Dickinson, Franklin Lakes, NJ, USA). Cultures were maintained in DMEM supplemented with 5 μg/mL gentamycin, 20 % plasma-derived bovine serum (First Link, Birmingham, UK), 1 ng/mL basic fibroblast growth factor (Roche Hungary, Budaörs, Hungary), and 100 μg/mL heparin. In the first 3 days, the culture medium contained puromycin (4 μg/mL) for the selective removal of P-glycoprotein-negative contaminating cells [33]. When brain endothelial cells in the dishes had become almost confluent, 550 nM hydrocortisone was added to the culture medium [32].

Cell cytotoxicity assays

Two tests were used to determine cell viability. In the colorimetric MTT assay, living cells convert the yellow dye 3-(4,5-dimethylthiazol-2-yl)-2,5-diphenyltetrazolium bromide (MTT) to purple, insoluble formazan crystals, and the number of metabolically active cells is proportional to the extent of formation of purple crystals. Confluent monolayers of rat brain endothelial cells in 96-well plates

were treated with precursor-derived $A\beta_{42}$ prepared in HCBS buffer as described above. After a 24-h treatment, the cells were incubated with 0.5 mg/mL MTT solution for 3 h in a CO_2 incubator. The formazan crystals were dissolved in DMSO and determined by measuring the absorbance at 570 nm with a microplate reader (Fluostar Optima, BMG Labtechnologies, Ortenberg, Germany).

The second method, real-time cell electronic sensing (RT-CES), is a label-free technique for the dynamic monitoring of living cells [34]. Special 96-well E-plates (Roche Hungary, Budaörs, Hungary) with gold electrodes at the bottom were coated with fibronectin and collagen type IV. Culture medium (50 μL) was added to each well for background readings. A rat brain endothelial cell suspension was dispensed at a density of 1.8×10^4 cells/well in 50 μL. The cells were kept in an incubator at 37 °C for 3 days, grew to confluency and reached a plateau phase of growth. On day 4, the cells were treated with peptide solution for 24 h as described above. The cell index was measured every 2 min, defined as $(R_n - R_b)/15$, where R_n is the cell-electrode impedance of the well containing cells and R_b is the background impedance of the well containing medium alone. In both assays, cells were treated with 10 mg/mL Triton X-100 detergent as a positive control for toxicity. The viability of cells was expressed as a percentage relative to control cells treated with buffer alone.

Statistical analysis

All data presented are mean ± SD. Comparisons were made by analysis of variance followed by the Newman–Keuls post hoc test using GraphPad Prism 5.0 software (GraphPad Software, La Jolla, CA, USA). Changes were considered statistically significant at $P < 0.05$. All experiments were repeated at least two times; the number of parallel wells for each treatment and time point varied between 4 and 6.

Results

Effects of Ca^{2+}/Mg^{2+} content of the buffer on the aggregation of native $A\beta_{42}$ and precursor-derived $A\beta_{42}$ monitored by ThT binding

The most convenient method to follow Aβ aggregation is the ThT-binding test [35]. When ThT binds to β sheet structures, a strong red shift can be detected in the fluorescence spectrum of the bound ThT as compared with that of the free molecule. We studied the effects of the buffer composition on the aggregation of native $A\beta_{42}$ and precursor-derived $A\beta_{42}$. Conventional HCO_3^--based buffer (HCBS) was used in our studies with physiological composition and pH that was prepared according to standard literature protocols.

The ThT assays revealed that the aggregation kinetics was highly dependent on the type and concentration of the peptide. The plain HCBS buffer (Fig. 2a) facilitated the formation of β-sheets of both peptides, with a greater effect on precursor-derived $A\beta_{42}$ oligomers. Divalent metal ions, such as Ca^{2+} and Mg^{2+}, can alter the structure of the peptide by influencing the secondary structure through interactions with negatively charged side chains. Figure 2b demonstrates the behavior of the peptides in HCBS with Ca^{2+} and Mg^{2+} according to their propensity toward forming β-sheets. The native $A\beta_{42}$ oligomers possessed an elevated ThT signal intensity, while the precursor-derived $A\beta_{42}$ oligomers showed only a moderate change in the signal intensity over time. By comparing the results depicted in Fig. 2a, b, it is obvious that in the presence of bivalent metal ions the ThT signal increased in the case of native $A\beta_{42}$ and decreased for precursor-derived $A\beta_{42}$. This indicates higher and lower beta sheet content in the aggregates, respectively.

Physicochemical investigation of the effects of Ca^{2+} and Mg^{2+} on the aggregation pathway: TEM and ECD studies

To elucidate the causes underlying the differences in the aggregation behavior of the peptides in the presence or absence of divalent metal ions, structural changes were studied by means of TEM and ECD spectroscopy.

The differences in the morphology of the peptide aggregates at a supramolecular level were monitored by TEM. Images in Fig. 3 depict the most abundant forms in the samples after 168 h of incubation. The presence of fibrillar superstructures formed in three cases indicates an ongoing transition from random/helical form to β-pleated, ordered aggregates. Native $A\beta_{42}$ incubated in HCBS in the absence of Ca^{2+} and Mg^{2+} (Fig. 3a) formed mature fibrils 5–6 nm in diameter. Determination of length was difficult because the curly aggregates tended to adhere together in bundles (Fig. 3a, inset), which might indicate a fibrilization pathway different from that experienced under physiological conditions (i.e., in the presence of bivalent metal ions). In contrast, Ca^{2+} and Mg^{2+} facilitated the formation of 'convenient' mature fibrils from native $A\beta_{42}$ units (Fig. 3b). These fibrils had a smooth surface, they were sometimes twisted, and their formation started from 'seeds' (aggregation centers), which could be unequivocally identified in the image (Fig. 3b, inset). The length of these fibrils at times exceeded 1–2 μm. A considerable number of protofibrils (up to 200 nm in length) were also present.

When incubated in HCBS (Fig. 3c), precursor-derived $A\beta_{42}$ formed regular mature fibrils (oligomers can be seen

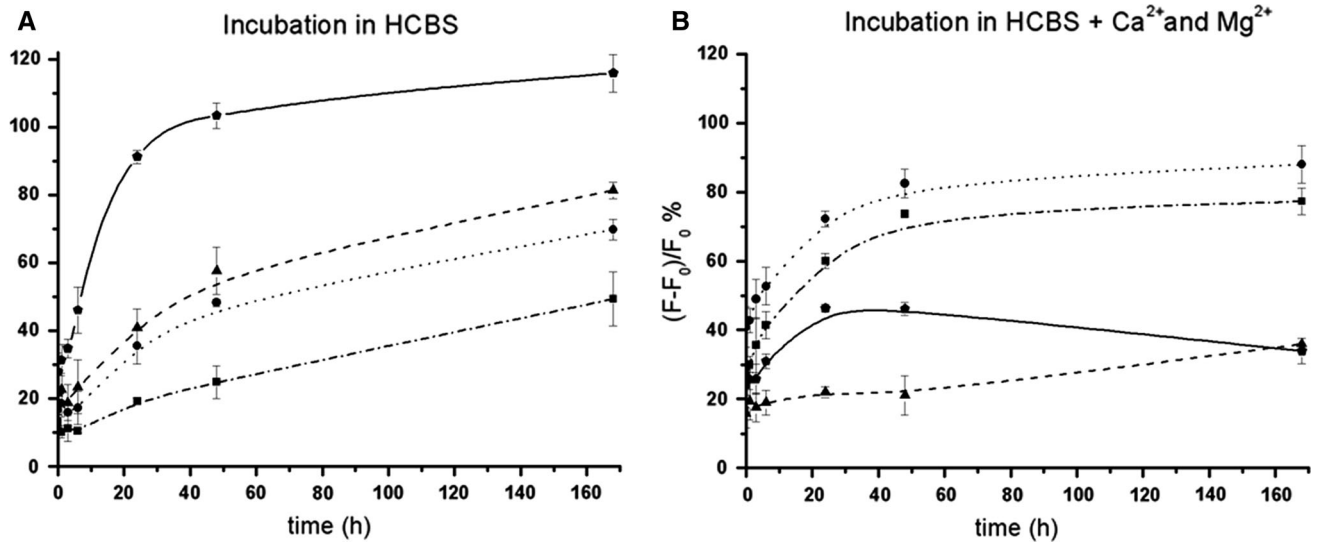

Fig. 2 β-sheet formation of Aβ in HCBS (A) and in HCBS + Ca^{2+}/Mg^{2+} (B), monitored by ThT binding. *Square with dashed dotted line* native $A\beta_{42}$ 25 μM, *diamond with dotted line* native $A\beta_{42}$ 75 μM, *triangle with dashed line* precursor-derived $A\beta_{42}$ 25 μM, *circle with solid line* precursor-derived $A\beta_{42}$ 75 μM

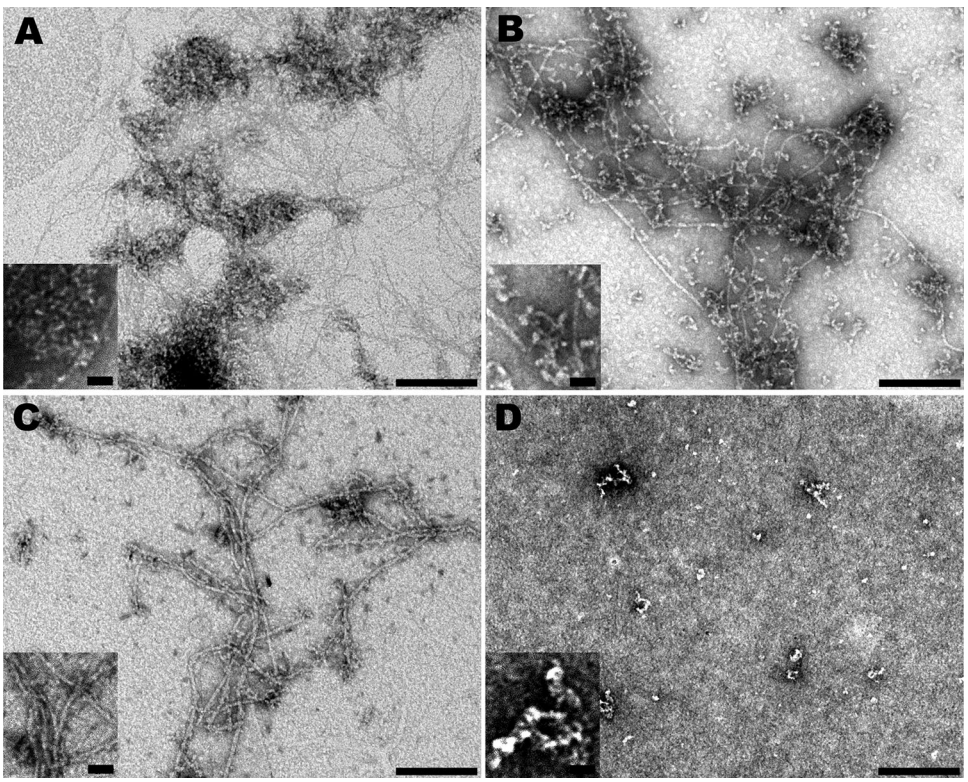

Fig. 3 TEM images of aggregates after incubation for 168 h at 37 °C. **a** native $A\beta_{42}$ in HCBS, 75 μM; **b** native $A\beta_{42}$ in HCBS + Ca^{2+} and Mg^{2+}, 75 μM; **c** precursor-derived $A\beta_{42}$ in HCBS, 75 μM; **d** precursor-derived $A\beta_{42}$ in HCBS + Ca^{2+} and Mg^{2+}, 75 μM. *Scale bars* 100 nm (full image) and 20 nm (*inset*)

scattered evenly in the background of the image as well), but there was no extensive formation of protofibrils (Fig. 3c, inset).

The most dramatic effect of the buffer composition on the aggregation pathway was experienced when precursor-derived $A\beta_{42}$ was incubated in HCBS with Ca^{2+} and

Mg^{2+}. The formation of regular β-sheeted structures was hindered, which manifested in the total absence of fibrillar aggregates (Fig. 3d). Small oligomers and irregularly shaped protofibrils resembling beaded chains predominated in the sample (Fig. 3d, inset).

To support our observation of the unexpected behavior of precursor-derived $A\beta_{42}$ in the presence of Ca^{2+} and Mg^{2+} ions shown by ThT binding and TEM investigations, we recorded the ECD spectra of this Aβ form in the absence and presence of Ca^{2+} and Mg^{2+} ions over a 1-week period (see Fig. 4). The peptide and salt concentrations applied did not allow data point collection below 200 nm. A strong minimum at 200 nm spanning to 230 nm indicated the presence of a mixture of random and β-sheet structures immediately after dissolution of the sample. A gradual decrease in the random contribution at 200 nm and an increase in the β-sheet signal component at 215 nm were observed in both cases (Fig. 4a, b) during the 1-week period.

The spectra of precursor-derived $A\beta_{42}$ solutions revealed a significant β-sheet character after incubation for 6 h (Fig. 4a, b). The gradual changes in the spectra both in the absence (Fig. 4a) and in the presence (Fig. 4b) of Ca^{2+} and Mg^{2+} indicated the slow transformation of random coil structures to β-sheet. However, the most pronounced changes were observed only after incubation for 48 h. Precursor-derived $A\beta_{42}$ in pure HCBS buffer displayed a strong minimum at 215 nm, while the minimum at 200 nm was greatly diminished, indicating virtually complete transformation to the β-sheet structure. In the presence of Ca^{2+} and Mg^{2+}, the β-sheet characteristics of the spectra were less pronounced even after 168 h, as the minimum at 215 nm was less intense than that in the absence of Ca^{2+} and Mg^{2+}. Thus, Ca^{2+} and Mg^{2+} significantly delayed or modulated the aggregation of precursor-derived $A\beta_{42}$ oligomers, as in contrast to results obtained in the absence of Ca^{2+} and Mg^{2+}, here only a slower, gradual decrease in the signal arising from unordered structures was observed.

Comparison of the effects of different $A\beta_{42}$ aggregates in biological studies

In order to reveal the relationship between the aggregation and the biological effectiveness, the peptide aggregates were tested in viability experiments using cell cultures. Besides a traditional endpoint test, we applied a new method, RT-CES, which monitors cell-substrate impedance for the noninvasive quantification of adherent cell proliferation and viability in real time [34]. Cells were seeded on E-plates containing microelectronic sensor arrays. The interaction between the cells and the electrode generates an impedance response that correlates linearly with the cell index, reflecting cell number, adherence, and cell growth [36]. RT-CES provides kinetic analysis with enhanced sensitivity relative to convenient colorimetric assays. The technique is therefore widely applied to test the effects of exogenous substances on the cell viability parameters. The results of a standard MTT test and RT-CES are compared in Fig. 5 to demonstrate the correlation between the two methodologies. Brain endothelial cell cultures were treated with iso-Aβ-derived oligomers in 50 μM concentration in both cases. After 24 h, a significant decrease in MTT reduction activity was observed (Fig. 5a, 69.9 % cell viability relative to control). In accord with this, the toxic effect of precursor-derived $A\beta_{42}$ treatment can be followed as a decrease in cell index in the sensogram, which is

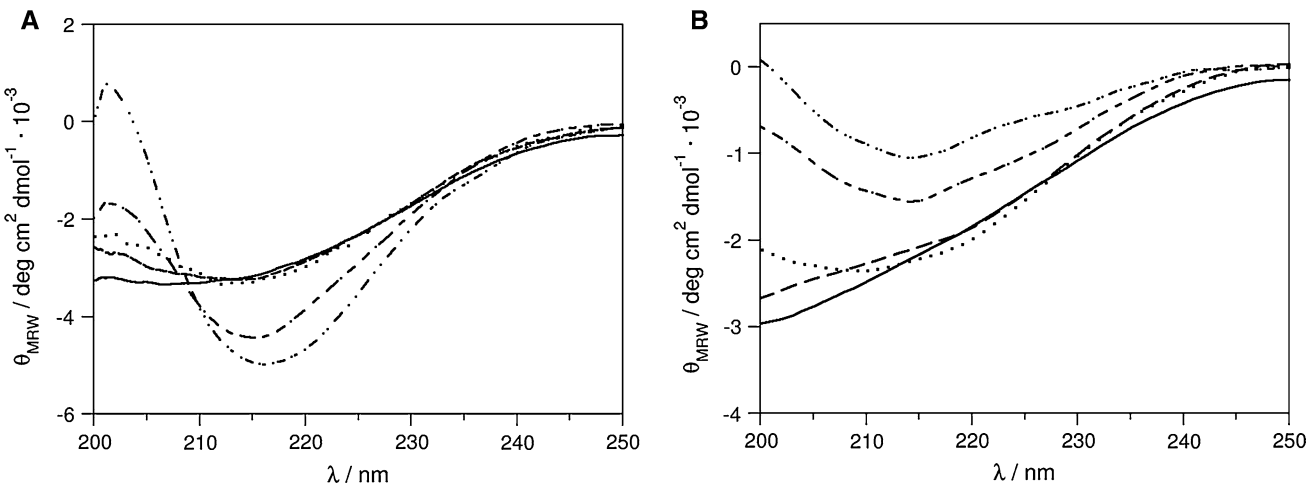

Fig. 4 ECD spectra of precursor-derived $A\beta_{42}$ (12.5 μM) in HCBS (**a**) and in HCBS + Ca^{2+}/Mg^{2+} (**b**) recorded immediately after peptide dissolution (*solid line*), and after incubation for 1 h (*dashed line*), 6 h (*dotted line*), 48 h (*dashed with single dotted line*), or 168 h (*dashed with double dotted line*) at 37 °C

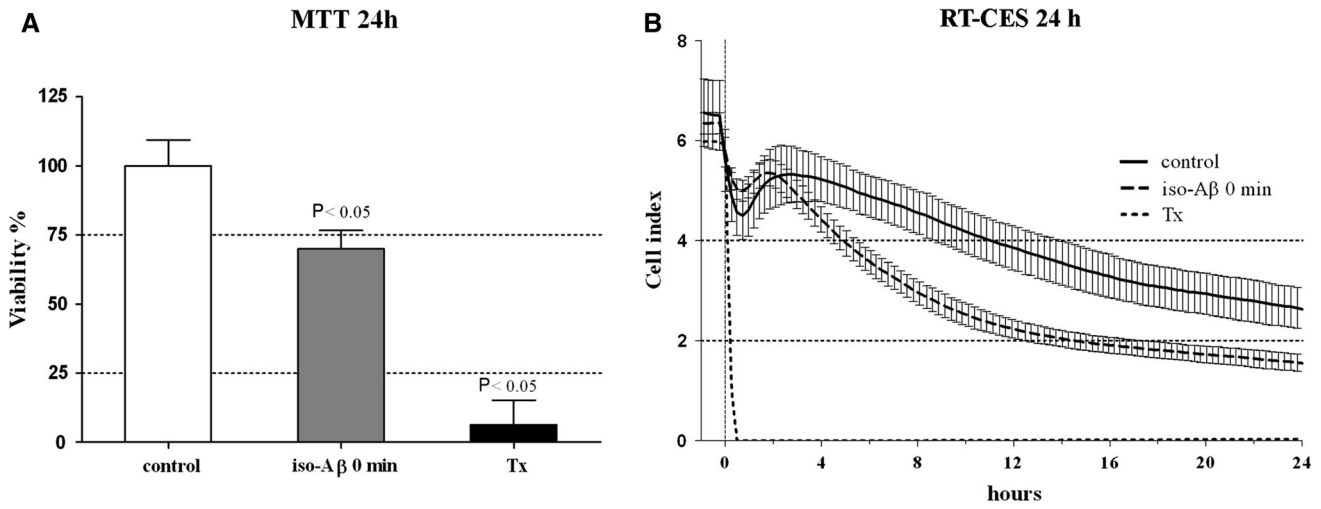

Fig. 5 Comparison of the colorimetric endpoint MTT viability assay and the real-time cell microelectric sensing method (RT-CES). Primary brain endothelial cells were treated with precursor-derived $A\beta_{42}$ in 50 μM final concentration for 24 h. MTT was assayed after this incubation period, while RT-CES was monitored constantly. T_x data represent the negative control measurements applying Triton X-100 to the cells

significant after 4 h (Fig. 5b). It can be stated that after the first perturbance caused by the medium change on all cells, the cell index increased close to the starting level (recovery phase), and then started to decline slowly, as the viability of the cells decreased. As compared with the control cells, Aβ treatment resulted in a significant cell index reduction, which lasted until the endpoint of the measurement. Treatment with Triton X-100 detergent (T_x) killed all the cells in both assays.

Brain endothelial cells were cultured in an E-plate and treated for 24 h with either native or precursor-derived $A\beta_{42}$ oligomers, in the presence or absence of Ca^{2+} and Mg^{2+} (Fig. 6). In order to compare the effects of the aggregation grade on the toxicity, the peptides were applied either without preincubation or after incubation for 24 h at 37 °C. The results demonstrate that the viability functions of the primary cells measured by RT-CES were significantly impaired by the amyloid treatment, in complete agreement with our previous data [22]. This experiment also revealed differences between the effects of the peptide preparations. Freshly prepared solutions possessed a pronounced toxicity regardless of their origin or the presence of Ca^{2+} and Mg^{2+}. On the other hand, incubation for 24 h caused a dramatic change in the toxicity of the different preparations. The highest effect was achieved by aggregating precursor-derived $A\beta_{42}$ in HCBS without Ca^{2+} and Mg^{2+} for 24 h (a drop in cell viability to 37.1 ± 2.3 % of the control). With this buffer, moderate toxicity was attained with fresh native $A\beta_{42}$ and precursor-derived $A\beta_{42}$ oligomers (native $A\beta_{42}$ in HCBS 53.2 ± 8.3 %, precursor-derived $A\beta_{42}$ in HCBS 58.8 ± 6.3 % viability relative to the control), while native $A\beta_{42}$-derived 24-h aggregates were the least toxic (68.0 ± 3.5 % viability). In the presence of Ca^{2+} and Mg^{2+}, the peptide preparations without preliminary incubation possessed comparable toxicity to that in the absence of the ions (native $A\beta_{42}$ 63.2 ± 7.9 %, precursor-derived $A\beta_{42}$ 67.7 ± 4.7 %), while both native and precursor-derived $A\beta_{42}$ aggregates exhibited a significantly decreased toxic effect after 24-h preincubation (native $A\beta_{42}$ 93.6 ± 9.9 %, precursor-derived $A\beta_{42}$ 79.5 ± 8.0 % cell viability).

Simulation of the secondary structures of native $A\beta_{42}$ and iso-$A\beta_{42}$ monomers by REMD

The aggregation pathway of the $A\beta_{42}$ is deeply influenced by the physico-chemical environment as it was already mentioned earlier. Among these, the initial conformational ensemble that is present in the solution is an important factor. After the addition of the buffer and setting the pH to the physiological value, iso-$A\beta_{42}$ transforms to the native Aβ form. The fact that the native and precursor-derived $A\beta_{42}$ become chemically identical this way and they are applied using uniform protocols afterward suggest that dissimilarities in their aggregation may originate from the differences in the initial conformational ensembles of the two peptides evolving during the synthetic preparation phase. In our experimental setup, these differences formed most probably during the HFIP treatment after the purification of the post-synthetic Aβ forms under acidic conditions. Therefore, REMD simulations were performed in order to identify these structural differences between the monomeric forms of native $A\beta_{42}$ and iso-$A\beta_{42}$ in solvent TFE (as a simple substituent of HFIP) at acidic pH of 2.0,

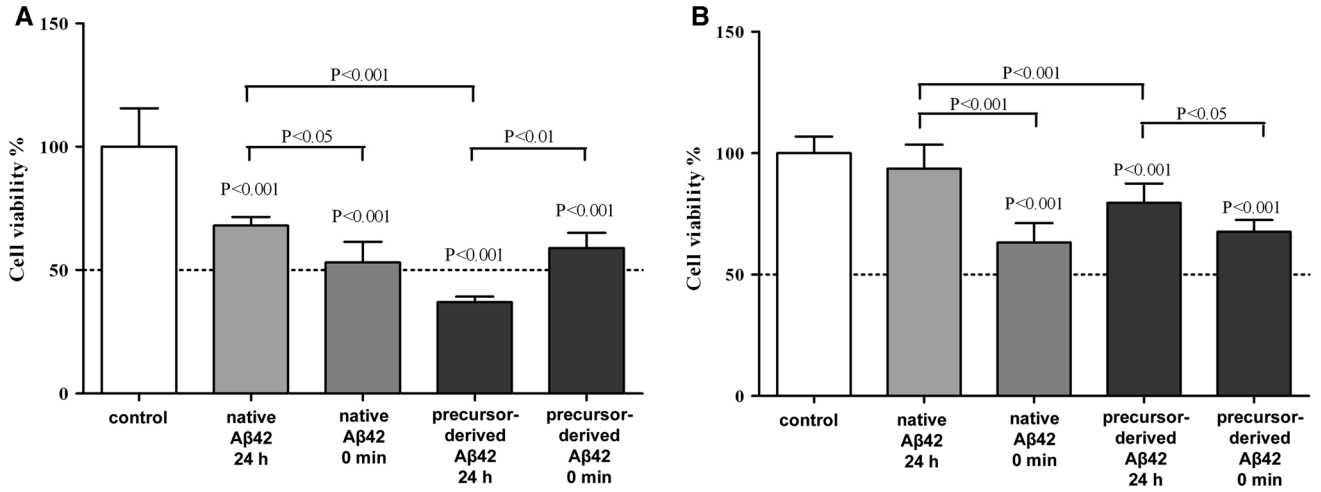

Fig. 6 Comparison of effects of $A\beta_{42}$ peptides on the viability of brain endothelial cells measured by RT-CES. Cells were treated with either native or precursor-derived $A\beta_{42}$ oligomers. Peptide solutions were prepared in 75 μM initial concentration and added to the cells immediately or after incubation for 24 h at 37 °C. Prior to administration, peptide stock solutions were diluted with cell culture medium to a final concentration of 50 μM. **a** $A\beta_{42}$ peptides dissolved in HCBS; **b** $A\beta_{42}$ peptides dissolved in HCBS containing Ca^{2+} and Mg^{2+}

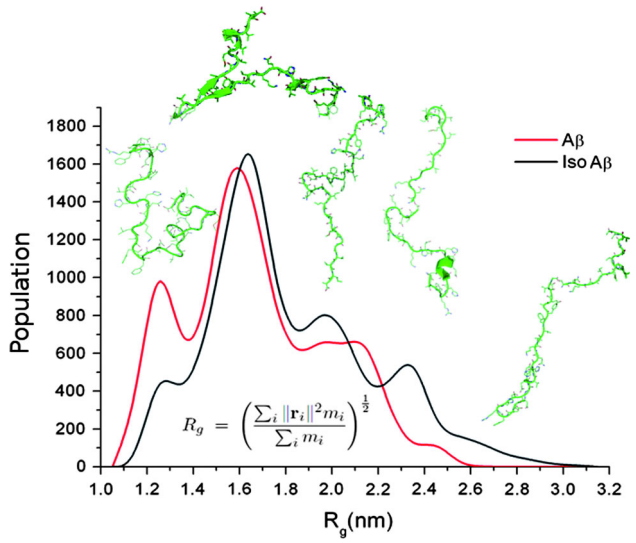

Fig. 7 Distribution of the calculated radius of gyration values for $A\beta_{42}$ and iso-$A\beta_{42}$ conformers obtained from the REMD simulation

which may provide explanation for their different aggregation properties in the presence of Ca^{2+} and Mg^{2+} in aqueous buffer.

Using the conformational ensemble obtained, we characterized the compactness of the monomeric Aβ conformers that were present in the TFE solution. Figure 7 presents the distribution curve of the calculated radius of gyration values for $A\beta_{42}$ and iso-$A\beta_{42}$ conformers obtained from the REMD simulation. The main difference between the distributions is that the iso-$A\beta_{42}$ curve is shifted toward the larger R_g values. Iso-$A\beta_{42}$ has a smaller number of compact conformers with the R_g value around 1.2 nm and larger number of extended structures ($R_g > 2.3$ nm).

Table 1 Relative frequencies of occurrence of the most populated secondary structural elements for native $A\beta_{42}$ and iso-$A\beta_{42}$ in the last 50 ns of the 300 K replica of the REMD simulation

Structural element	native $A\beta_{42}$ (%)	iso-$A\beta_{42}$ (%)
β-strand	8.3	10.1
β-turn	8.0	7.8
α-helix	1.6	5.7
3_{10} helix	3.6	3.7

Table 1 presents relative frequencies of occurrence of the secondary structural elements for the complete sequence of native $A\beta_{42}$ and iso-$A\beta_{42}$ monomers. There is no fundamental difference between the investigated peptides. The appearance of secondary structural elements is very rare for both peptides; only β-strand and turn structures have been found to account for more than 7 % of the total population. Thus, the peptides had dominantly unordered structures during our simulations. In spite of the low average appearance of the secondary structural motifs, local structural preferences and their differences may give additional details to the global picture. Figure 8 presents the distributions of the relative frequency of occurrences of four common secondary structural elements along the sequence of native and iso-$A\beta_{42}$. Although these distributions show high similarity, the residues Ser^{8}–Glu^{11} of iso-$A\beta_{42}$, close to the N-terminal end, show higher propensity of having helical structure. The distributions of β-turn and β-strand conformations are somewhat different in this

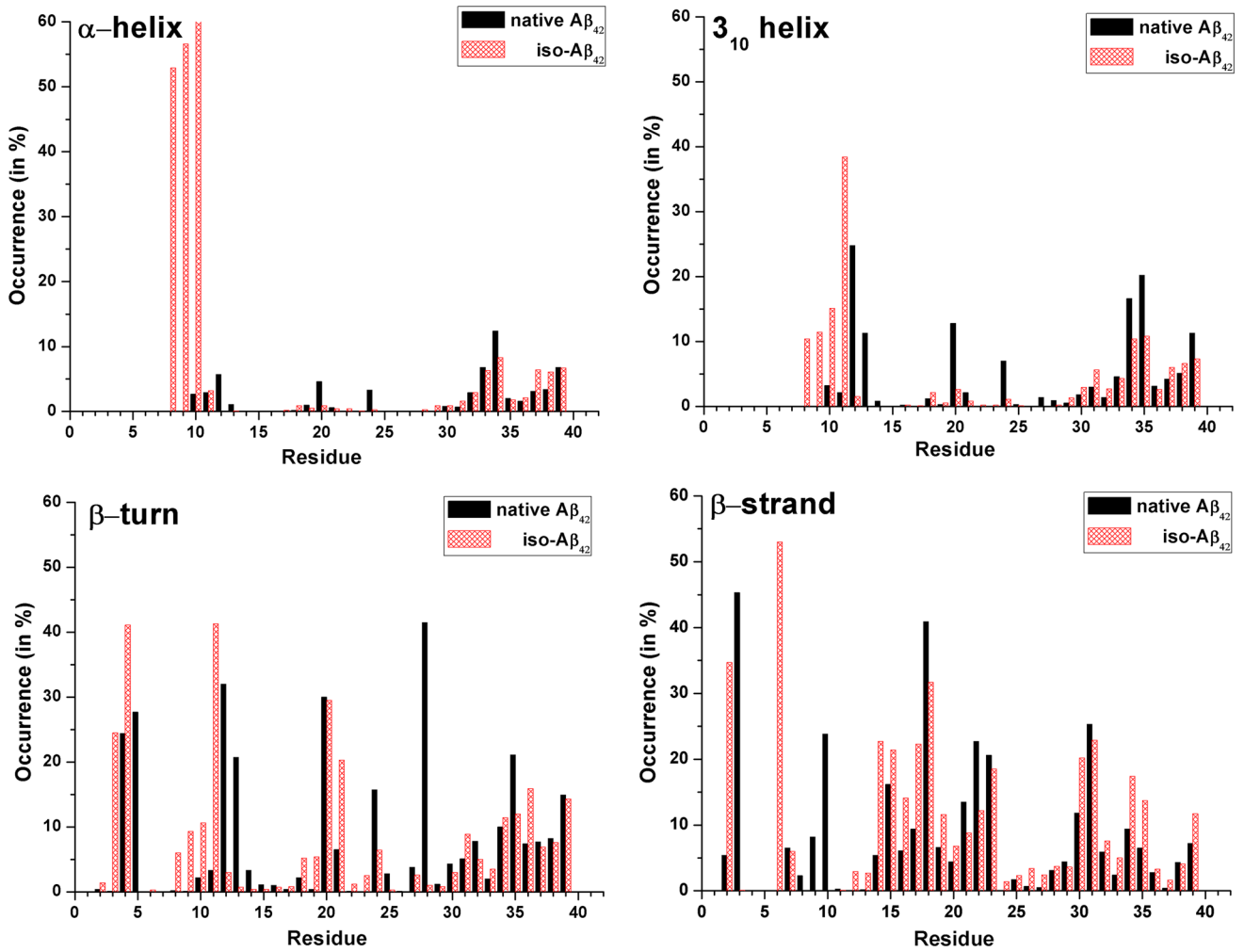

Fig. 8 Relative frequencies of occurrence of the most populated secondary structural elements along the sequences of native $A\beta_{42}$ and iso-$A\beta_{42}$ in the last 50 ns of the 300 K replica of the REMD simulation

region, as well. It is worth also to mention that the turn appears near the residue Lys^{28} in the case of native $A\beta_{42}$ almost completely missing in the other case.

There are several hypotheses for early folding contacts, between amino acids of Aβ providing toxic oligomers [37]. The salt bridge formed by Asp^{23} and Lys^{28} in $A\beta_{42}$ plays a crucial role in the process of Aβ aggregation [38]. The depsipeptide bond between Gly^{25} and Ser^{26} in iso-$A\beta_{42}$ makes the backbone between the two salt bridge-forming amino acids distorted, which hinders the formation of this important structural element. Table 2 lists the relative frequencies of occurrence of some important H-bonds formed by Lys^{28} as donor for the investigated peptides in the last 50 ns of the 300 K assembly of the simulation. We can see that H-bonds formed by the Lys^{28} side chain as donor are reduced in iso-$A\beta_{42}$ as compared with native $A\beta_{42}$. Numerous H-bonds were detected between Lys^{28} and the main chain carbonyl group of Asn^{27} in native $A\beta_{42}$ (44.1 %). Besides this highly populated conformation, there is a considerable amount (21.1 %) of H-bonds between Lys^{28} and Asp^{23}. In iso-$A\beta_{42}$, the population of H-bonds with Val^{24} and Asp^{23}, situated on the other side of the depsipeptide bond, is considerably decreased (2.6 %).

Table 2 Relative frequency of occurrence of the most populated H-bonds formed by the Lys^{28} side chain as donor for native $A\beta_{42}$ and iso-$A\beta_{42}$ in the last 50 ns of the 300 K replica of the simulation

Acceptor	native $A\beta_{42}$ (%)	iso-$A\beta_{42}$ (%)
Asn^{27} side chain	44.1	12.3
Asn^{27} main chain	9.1	13.5
Ser^{26} main chain	26.2	43.9
Ser^{26} side chain	21.6	0.0
Val^{24} main chain	21.2	2.0
Asp^{23} side chain	21.1	2.6

In this way, the specific conformation of the Lys^{28} Asp^{23} residue pair that can be transformed to the salt bridge by pH switching is not favored in iso-$A\beta_{42}$.

The carboxylate groups of the acidic residues Glu and Asp are potential binding sites for divalent metal ions. We investigated the occupancy of these side chain functions, assuming that their cation-binding propensities are hindered if they form H-bonds with other residues. We calculated therefore the average numbers of H-bonds formed by the carboxylate groups of the acidic residues of the peptides (Table 3). Comparison of the data revealed that carboxylates at the N-terminal end are less occupied by H-bonds in native $A\beta_{42}$ than in iso-$A\beta_{42}$, whereas an opposite tendency is observed for the residues in the fibril-forming region (the hairpin region).

Discussion

The 'amyloid challenge'

The use of exogenous Aβ in experiments poses many difficulties from the very beginning. It has become clear that the amyloidogenic polypeptides can produce both toxic and non-toxic oligomeric forms [39, 40]. The heterogeneity and unstable nature of the naturally occurring oligomeric intermediates make it difficult to define their conformational transitions and discern the physico-chemical properties that correlate with toxicity [41]. In fact, to fully understand the Aβ toxicity, it would be essential to solve the 3D structure of early oligomers as they provide insights into molecular interactions. Despite the limitations (e.g., sensitivity) of solution NMR measurements, recently the high resolution structures of $A\beta_{40}$ [42] as well as $A\beta_{42}$ [43] were determined by NMR techniques.

An enormous amount of information has already been gathered concerning the utilization and characterization of the Aβ peptide. The number of standardized utilization protocols is constantly increasing, which makes a decision as to the best one almost impossible [10]. The quality and properties of synthetic Aβ exhibit great batch-to-batch variability, and the basis of the protocols is therefore always an initial pretreatment, whereby the different Aβ preparations can be converted to a uniform, soluble state.

Neither a solubilizing agent nor a treatment with basic solution was proven to break the post-synthetic conformation and aggregation grade of Aβ completely. Therefore, various separation techniques (centrifugation, filtration or size exclusion chromatography) are extensively applied to remove the insoluble part of the peptide.

To overcome this problem, a new synthesis method, the depsipeptide method, was elaborated for $A\beta_{42}$ synthesis [14, 15]. We previously reported [16] that the depsipeptide derivative of $A\beta_{42}$, termed iso-$A\beta_{42}$, could be synthetized with fewer problems and with solution properties more advantageous relative to synthetic native $A\beta_{42}$. The ester bond in iso-$A\beta_{42}$ causes bending of the peptide backbone as compared to native $A\beta_{42}$, and aggregation of the peptide chains during synthesis is therefore less favored. The ester bond is stable at acidic pH, the peptide can be dissolved in pure Milli Q water to a relatively high concentration (100 μM), and this stock can be utilized for sample preparation for days without any detectable sign of aggregation. We have found, however, that the depsipeptide is still able to form small protofibrillar assemblies during the post-synthetic purification process, presumably because of the exposed hydrophobic surfaces of the peptide chain, though to a much lower extent than for native $A\beta_{42}$ [16]. We therefore use HFIP treatment before preparation of the stock solution in order to break up these partially folded aggregates.

Table 3 Average numbers of H-bonds formed by the carboxylate groups at given positions with any other residues of native $A\beta_{42}$ and iso-$A\beta_{42}$ in the last 50 ns of the 300 K replica of the simulation

	native $A\beta_{42}$	iso-$A\beta_{42}$
Asp^{1}	1.5	**3.1**
Glu^{3}	1.7	**2.7**
Asp^{7}	**3.9**	2.6
Glu^{11}	**3.3**	1.7
Glu^{22}	**3.2**	1.6
Asp^{23}	**3.6**	1.8
Ala^{42}-OH	**1.7**	1.3

Bold numbers indicate the larger values of the matched data pairs

Sensitivity of the aggregation process on the Ca^{2+}/Mg^{2+} content of the buffer

The application of standardized protocols from the literature may involve the drawback that sometimes the protocol cannot be fitted to the experimental setups routinely used in the laboratory. Many groups therefore attempted to combine given preparation prescriptions with their own protocols. Our results clearly demonstrate that extreme care must be taken when accepted protocols are changed. Even factors that may appear insignificant regarding the handling of the peptide can have dramatic effects on the aggregation pathway. Buffer supplements, e.g., nutritional elements, antibiotics, specific ions, and complexing agents, can all influence the aggregation, with changes in the size distribution, morphology, and secondary structure of the oligomers.

In our present study, it was experienced that native $A\beta_{42}$ and precursor-derived $A\beta_{42}$ possess distinct aggregation characteristics, already in HCBS buffer without additional metal ions. ThT measurements show a higher β-sheet content for precursor-derived $A\beta_{42}$ in the early as well as the later phase of aggregation β. TEM images indicate also morphological dissimilarities of the aggregates formed from the two Aβ forms in HCBS after 168 h of incubation. The reason may originate from the differences in the conformational ensembles formed during the preparation process that was found in our REMD simulations. The native $A\beta_{42}$ has fewer of the extended (with larger radius of gyration) and more of the compact (with smaller radius of gyration) conformations initially than the precursor-derived $A\beta_{42}$. This way, the latter can form more of those oligomers already at the early stage of the aggregations process that are able to evolve in the direction of fibril formation. On the other hand, the native $A\beta_{42}$ having more of the compact monomer structures probably forms more of the conformers incompatible with the fast fibril formation pathway (see upper part of Fig. 9).

By adding Ca^{2+} and Mg^{2+} ions to the buffer, a strong modulating effect could be observed. These ions are common ingredients of most physiological buffers. Regarding the aggregation pathway of $A\beta_{42}$, Ca^{2+} may be more important than Mg^{2+} for two reasons: (1) Ca^{2+} is usually applied in a higher concentration and (2) the ability of Ca^{2+} to bind to specific side chain functions of amino acids is more pronounced than that of Mg^{2+}.

Interestingly, the ions had opposite effects on the aggregation of the two peptides as it was shown by ThT-binding measurements. The formation of β-sheets of native $A\beta_{42}$ oligomers was facilitated in the presence of Ca^{2+} and Mg^{2+}, while they strongly inhibited the aggregation of precursor-derived $A\beta_{42}$. These findings were supported by ECD measurements, which revealed marked hindrance of the unordered → β-sheet conversion, in the case of precursor-derived $A\beta_{42}$. Moreover, significant differences in the morphology of the aggregates were detected by TEM, in agreement with the observed inhibition by Ca^{2+} and Mg^{2+} of the aggregation of precursor-derived $A\beta_{42}$.

The biological consequences of the structural differences of the $A\beta_{42}$ oligomers were also studied in viability experiments with cell cultures, where the cells were exposed directly to the aggregates. We recently published the results of toxicity studies of native $A\beta_{42}$ on primary rat brain endothelial cells co-cultured with rat glial cells [22, 23]. A previous investigation [44] and our data prove that brain microvessel endothelial cells are definitely sensitive to toxic $A\beta_{42}$. In the absence of Ca^{2+} and Mg^{2+}, preliminary aggregation helped to enhance the toxicity of precursor-derived $A\beta_{42}$, probably by making the formation of a putative toxic conformation possible. The decrease in the efficacy of native $A\beta_{42}$ may be explained by the sluggish

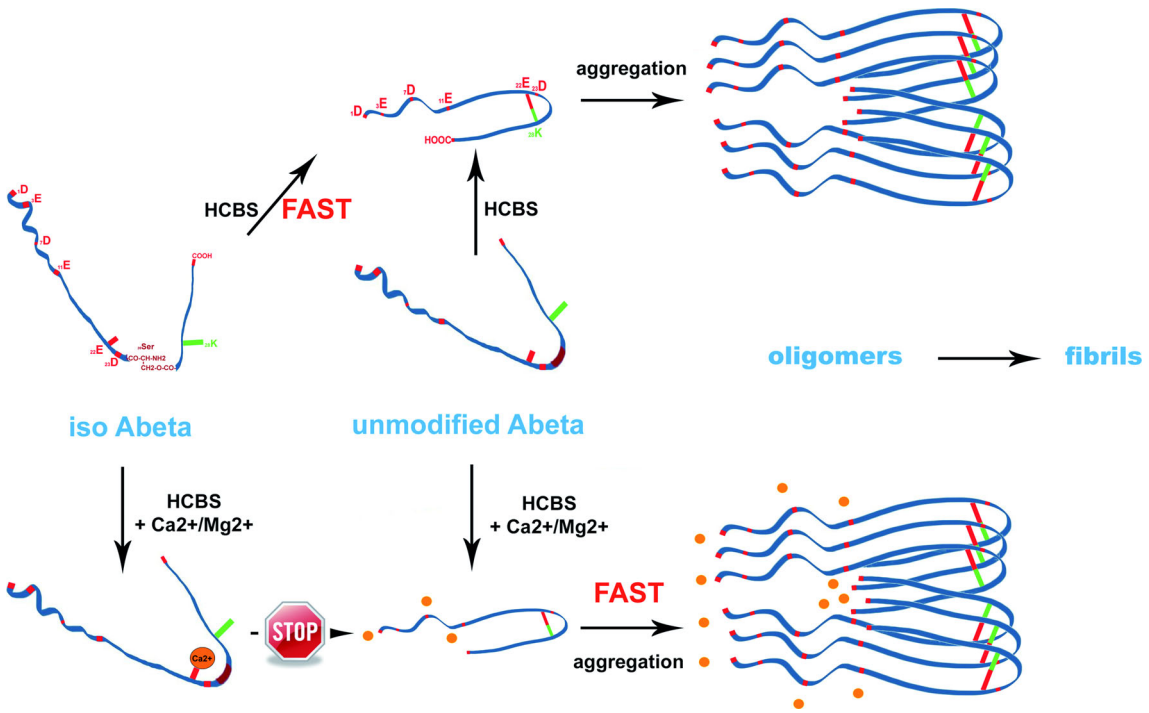

Fig. 9 Model of aggregation pathways of native $A\beta_{42}$ and precursor-derived $A\beta_{42}$ in the absence (*upper part*) and in the presence (*lower part*) of Ca^{2+} and Mg^{2+} ions

formation of the toxic oligomers relative to those of precursor-derived $A\beta_{42}$. Literature data demonstrate that conserved features of intermediates in several amyloid assemblies determine their benign or toxic states. Less compact, more hydrophobic oligomers with intrinsically disordered structures were toxic and the more compact, less hydrophobic oligomers proved to be non-toxic [41]. In our experiments, the effects of the metal ions could be observed as a loss of activity in case of both Aβ peptide types. The increased aggregation of native $A\beta_{42}$, observed in the physico-chemical studies, may result in an ordered structure and a massive decrease in the toxicity of native $A\beta_{42}$. The increased rate of aggregation led to the formation of large aggregates, with ordered structure decreasing both the effective surface and the diffusion ability.

Decreased activity of precursor-derived $A\beta_{42}$ oligomers can be explained with the aggregation inhibiting effect of the metal ions. However, this phenomenon was not terminal, as it was demonstrated by the toxicity data of both the pre-aggregated and fresh precursor-derived $A\beta_{42}$, where a considerable level of toxicity was measured despite the Ca^{2+} and Mg^{2+} content of the cell-culturing medium. The observed phenomenon may serve as a good model for the slow progression of AD. Physiological Ca^{2+} and Mg^{2+} concentrations might slow down the formation of toxic Aβ aggregates from the originally unordered APP-derived $A\beta_{42}$ monomers, and that would lead to the slow pathophysiological progress of AD.

How can Ca^{2+} and Mg^{2+} influence the aggregation pathways of the different Aβ types?

It is known from the literature that Ca^{2+} in physiological concentration facilitates the aggregation of native $A\beta_{42}$. Fluorescence photobleaching recovery has revealed that, up to a concentration of 15 mM, Ca^{2+} enhances the aggregation of native $A\beta_{42}$ oligomers [45]. Similar results were achieved in size exclusion chromatography, ThT and ECD experiments, where it was found that the fibril formation of native $A\beta_{42}$ was accelerated by a physiological (2 mM) concentration of Ca^{2+} [19] in good accord with our findings. It was assumed that Ca^{2+} binding to the side chain functions in the more flexible N-terminal region provides rigidity and consequently facilitates fibril formation. This is in good agreement with our REMD results, indicating that the N-terminal side chain carboxylates are less involved in H-bonding and therefore more prone to complexation by Ca^{2+} and Mg^{2+} (see lower part of Fig. 9).

On the basis of solid-state NMR data, Sciarretta et al. [38] proposed that the salt bridge formation between Asp^{23} and Lys^{28} is the rate-limiting step in fibrillogenesis. Their findings were supported by molecular dynamics simulations [46]. As our simulations showed, conformations with an H-bond between the bridge residues which can therefore be regarded as precursors in the fibrilization pathway are present in native $A\beta_{42}$, but completely absent from precursor-derived $A\beta_{42}$. After the acyl shift, precursor-derived $A\beta_{42}$ also has a possibility to form a salt bridge, if external effects do not inhibit this. Consequently, insertion of Ca^{2+} and Mg^{2+} into the turn-forming region by complex binding to the less-occupied carboxylates in precursor-derived $A\beta_{42}$ may exert such an inhibitory effect (see lower part of Fig. 9).

Conclusions

Use of the depsipeptide iso-$A\beta_{42}$ as $A\beta_{42}$-precursor in biological experiments instead of synthetic Aβ eliminates most of the problems related to the sample preparation and the synthetic origin of the peptide. In our studies, these two Aβ forms showed high similarity in their biological effects, as well as in their main structural characteristics under well-chosen experimental circumstances. However, the aggregation properties of these two Aβ forms showed high sensitivity on deviation from these prescriptions that may manifest in different aggregation pathways and biological effects. Namely, adding Ca^{2+} and Mg^{2+} to the buffer facilitated the aggregation of native $A\beta_{42}$, resulting in aggregated species with decreased toxicity. On the contrary, aggregation to fibrils of precursor-derived $A\beta_{42}$ was hindered by these divalent metal ions. The opposite influences were possibly due to the differences in the conformational ensembles evolved during the preparation process of the two Aβ forms as it was elucidated with the aid of REMD simulations. The different compositions of the conformational ensembles, initially present, led to different aggregation pathways if Ca^{2+} and Mg^{2+} were added to the buffer. These findings also support the intrinsically disordered character of $A\beta_{42}$ peptide [47].

Acknowledgments The research leading to these results has received funding from the European Community's Seventh Framework Program (FP7/2007-2013) under Grant agreements No. 201159 and No. 211696. LF and SV acknowledges the award of János Bolyai Fellowship from the HAS. This work was supported in part by grants of the Hungarian National Scientific Research Fund (OTKA K 101825). Research contribution of AB was supported by the European Union and the State of Hungary, co-financed by the European Social Fund in the framework of TÁMOP-4.2.4.A/2-11/1-2012-0001 'National Excellence Program.' Calculations were carried out on the computers of the Hungarian National Information Infrastructure Development Institute (NIIFI).

References

1. Hardy JA, Higgins GA (1992) Alzheimer's disease—the amyloid cascade hypothesis. Science 256(5054):184–185

2. Hardy J, Selkoe DJ (2002) Medicine—the amyloid hypothesis of Alzheimer's disease: progress and problems on the road to therapeutics. Science 297(5580):353–356. doi:10.1126/science.1072994
3. Walsh DM, Lomakin A, Benedek GB, Condron MM, Teplow DB (1997) Amyloid beta-protein fibrillogenesis—detection of a protofibrillar intermediate. J Biol Chem 272(35):22364–22372
4. Davis RC, Marsden IT, Maloney MT, Minamide LS, Podlisny M, Selkoe DJ, Bamburg JR (2011) Amyloid beta dimers/trimers potently induce cofilin-actin rods that are inhibited by maintaining cofilin-phosphorylation. Mol Neurodegener 6:16. doi:10.1186/1750-1326-6-10
5. Ono K, Yamada M (2011) Low-n oligomers as therapeutic targets of Alzheimer's disease. J Neurochem 117(1):19–28. doi:10.1111/j.1471-4159.2011.07187.x
6. Lesne S, Koh MT, Kotilinek L, Kayed R, Glabe CG, Yang A, Gallagher M, Ashe KH (2006) A specific amyloid-beta protein assembly in the brain impairs memory. Nature 440(7082):352–357. doi:10.1038/nature04533
7. Lambert MP, Barlow AK, Chromy BA, Edwards C, Freed R, Liosatos M, Morgan TE, Rozovsky I, Trommer B, Viola KL, Wals P, Zhang C, Finch CE, Krafft GA, Klein WL (1998) Diffusible, nonfibrillar ligands derived from A beta(1–42) are potent central nervous system neurotoxins. Proc Natl Acad Sci USA 95(11):6448–6453
8. Wang HW, Pasternak JF, Kuo H, Ristic H, Lambert MP, Chromy B, Viola KL, Klein WL, Stine WB, Krafft GA, Trommer BL (2002) Soluble oligomers of beta amyloid (1–42) inhibit long-term potentiation but not long-term depression in rat dentate gyrus. Brain Res 924(2):133–140
9. Teplow DB (2006) Preparation of amyloid beta-protein for structural and functional studies. In: Amyloid, prions, and other protein aggregates, Pt C, vol 413. Methods in enzymology, pp 20–33. doi:10.1016/s0076-6879(06)13002-5
10. Benilova I, Karran E, De Strooper B (2012) The toxic A beta oligomer and Alzheimer's disease: an emperor in need of clothes. Nat Neurosci 15(3):349–357. doi:10.1038/nn.3028
11. Lu J-X, Qiang W, Yau W-M, Schwieters CD, Meredith SC, Tycko R (2013) Molecular structure of beta-amyloid fibrils in Alzheimer's disease brain tissue. Cell 154(6):1257–1268. doi:10.1016/j.cell.2013.08.035
12. Tycko R, Wickner RB (2013) Molecular structures of amyloid and prion fibrils: consensus versus controversy. Acc Chem Res 46(7):1487–1496. doi:10.1021/ar300282r
13. Schuetz AK, Vagt T, Huber M, Ovchinnikova OY, Cadalbert R, Wall J, Guentert P, Boeckmann A, Glockshuber R, Meier BH (2015) Atomic-resolution three-dimensional structure of amyloid beta fibrils bearing the osaka mutation. Angew Chem Int Ed 54(1):331–335. doi:10.1002/anie.201408598
14. Carpino LA, Krause E, Sferdean CD, Schumann M, Fabian H, Bienert M, Beyermann M (2004) Synthesis of 'difficult' peptide sequences: application of a depsipeptide technique to the Jung-Redemann 10- and 26-mers and the amyloid peptide A beta(1–42). Tetrahedron Lett 45(40):7519–7523. doi:10.1016/j.tetlet.2004.07.162
15. Sohma Y, Sasaki M, Hayashi Y, Kimura T, Kiso Y (2004) Design and synthesis of a novel water-soluble A beta 1–42 isopeptide: an efficient strategy for the preparation of Alzheimer's disease-related peptide, A beta 1–42, via O-N intramolecular acyl migration reaction. Tetrahedron Lett 45(31):5965–5968. doi:10.1016/j.tetlet.2004.06.059
16. Bozso Z, Penke B, Simon D, Laczko I, Juhasz G, Szegedi V, Kasza A, Soos K, Hetenyi A, Weber E, Tohati H, Csete M, Zarandi M, Fulop L (2009) Controlled in situ preparation of A beta(1–42) oligomers from the isopeptide "iso-A beta(1–42)", physicochemical and biological characterization. Peptides 31(2):248–256. doi:10.1016/j.peptides.2009.12.001
17. Klement K, Wieligmann K, Meinhardt J, Hortschansky P, Richter W, Fandrich M (2007) Effect of different salt ions on the propensity of aggregation and on the structure of Alzheimer's A beta(1–40) amyloid fibrils. J Mol Biol 373(5):1321–1333
18. Isaacs AM, Senn DB, Yuan ML, Shine JP, Yankner BA (2006) Acceleration of amyloid beta-peptide aggregation by physiological concentrations of calcium. J Biol Chem 281(38):27916–27923
19. Ahmad A, Muzaffar M, Ingram VM (2009) Ca^{2+}, within the physiological concentrations, selectively accelerates A beta 42 fibril formation and not A beta 40 in vitro. Biochim Biophys Acta Proteins Proteomics 1794(10):1537–1548. doi:10.1016/j.bbapap.2009.06.022
20. Brannstrom K, Ohman A, Lindhagen-Persson M, Olofsson A (2013) Ca^{2+} enhances A beta polymerization rate and fibrillar stability in a dynamic manner. Biochem J 450:189–197
21. Smith MD, Cruz L (2013) Effect of ionic aqueous environments on the structure and dynamics of the A beta(21–30) fragment: a molecular-dynamics study. J Phys Chem B 117(22):6614–6624
22. Deli MA, Veszelka S, Csiszar B, Toth A, Kittel A, Csete M, Sipos A, Szalai A, Fulop L, Penke B, Abraham CS, Niwa M (2010) Protection of the blood-brain barrier by pentosan against amyloid-beta-induced toxicity. J Alzheimers Dis 22(3):777–794. doi:10.3233/jad-2010-100759
23. Veszelka S, Tóth AE, Walter FR, Datki Z, Mózes E, Fülöp L, Bozsó Z, Hellinger É, Vastag M, Orsolits B, Környei Z, Penke B, Deli MA (2013) Docosahexaenoic acid reduces amyloid-β induced toxicity in cells of the neurovascular unit. J Alzheimers Dis 36(3):487–501
24. Zarandi M, Soos K, Fulop L, Bozso Z, Datki Z, Toth GK, Penke B (2007) Synthesis of A beta(1–42) and its derivatives with improved efficiency. J Pept Sci 13(2):94–99. doi:10.1002/psc.801
25. Hukushima K, Nemoto K (1996) Exchange Monte Carlo method and application to spin glass simulations. J Phys Soc Jpn 65(6):1604–1608. doi:10.1143/jpsj.65.1604
26. Sugita Y, Okamoto Y (1999) Replica-exchange molecular dynamics method for protein folding. Chem Phys Lett 314(1–2):141–151. doi:10.1016/s0009-2614(99)01123-9
27. Duan Y, Wu C, Chowdhury S, Lee MC, Xiong GM, Zhang W, Yang R, Cieplak P, Luo R, Lee T, Caldwell J, Wang JM, Kollman P (2003) A point-charge force field for molecular mechanics simulations of proteins based on condensed-phase quantum mechanical calculations. J Comput Chem 24(16):1999–2012. doi:10.1002/jcc.10349
28. Hess B, Kutzner C, van der Spoel D, Lindahl E (2008) GROMACS 4: algorithms for highly efficient, load-balanced, and scalable molecular simulation. J Chem Theory Comput 4(3):435–447. doi:10.1021/ct700301q
29. Wang JM, Wolf RM, Caldwell JW, Kollman PA, Case DA (2004) Development and testing of a general amber force field. J Comput Chem 25(9):1157–1174. doi:10.1002/jcc.20035
30. Bayly CI, Cieplak P, Cornell WD, Kollman PA (1993) A well-behaved electrostatic potential based method using charge restraints for deriving atomic charges—the RESP model. J Phys Chem 97(40):10269–10280. doi:10.1021/j100142a004
31. Nagy G, Oostenbrink C (2014) Dihedral-based segment identification and classification of biopolymers I: proteins. J Chem Inf Model 54(1):266–277. doi:10.1021/ci400541d
32. Deli MA, Abraham CS, Kataoka Y, Niwa M (2005) Permeability studies on in vitro blood-brain barrier models: physiology, pathology, and pharmacology. Cell Mol Neurobiol 25(1):59–127
33. Perriere N, Demeuse PH, Garcia E, Regina A, Debray M, Andreux JP, Couvreur P, Scherrmann JM, Temsamani J, Couraud PO, Deli MA, Roux F (2005) Puromycin-based purification of rat brain capillary endothelial cell cultures. Effect on the expression of blood-brain barrier-specific properties. J Neurochem 93(2):279–289

34. Xia M, Huang R, Witt KL, Southall N, Fostel J, Cho MH, Jadhav A, Smith CS, Inglese J, Portier CJ, Tice RR, Austin CP (2008) Compound cytotoxicity profiling using quantitative high-throughput screening. Environ Health Perspect 116(3):284–291
35. LeVine H (1999) Quantification of beta-sheet amyloid fibril structures with thioflavin T. In: Amyloid, prions, and other protein aggregates, vol 309. Methods in enzymology, pp 274–284
36. Ozsvari B, Puskas LG, Nagy LI, Kanizsai I, Gyuris M, Madacsi R, Feher LZ, Gero D, Szabo C (2010) A cell-microelectronic sensing technique for the screening of cytoprotective compounds. Int J Mol Med 25(4):525–530
37. Das AK, Rawat A, Bhowmik D, Pandit R, Huster D, Maiti S (2015) An early folding contact between Phe19 and Leu34 is critical for amyloid-β oligomer toxicity. ACS Chem Neurosci. doi:10.1021/acschemneuro.5b00074
38. Sciarretta KL, Gordon DJ, Petkova AT, Tycko R, Meredith SC (2005) A beta 40-lactam(D23/K28) models a conformation highly favorable for nucleation of amyloid. Biochemistry 44(16):6003–6014. doi:10.1016/bi0474867
39. Campioni S, Mannini B, Zampagni M, Pensalfini A, Parrini C, Evangelisti E, Relini A, Stefani M, Dobson CM, Cecchi C, Chiti F (2010) A causative link between the structure of aberrant protein oligomers and their toxicity. Nat Chem Biol 6(2):140–147. doi:10.1038/nchembio.283
40. Glabe CG (2008) Structural classification of toxic amyloid oligomers. J Biol Chem 283(44):29639–29643. doi:10.1074/jbc.R800016200
41. Krishnan R, Goodman JL, Mukhopadhyay S, Pacheco CD, Lemke EA, Deniz AA, Lindquist S (2012) Conserved features of intermediates in amyloid assembly determine their benign or toxic states. Proc Natl Acad Sci USA 109(28):11172–11177. doi:10.1073/pnas.1209527109
42. Ramamoorthy A, Lim MH (2013) Structural characterization and inhibition of toxic amyloid-beta oligomeric intermediates. Biophys J 105(2):287–288. doi:10.1016/j.bpj.2013.05.004
43. Waelti MA, Orts J, Voegeli B, Campioni S, Riek R (2015) Solution NMR studies of recombinant a beta(1–42): from the presence of a micellar entity to residual beta-sheet structure in the soluble species. ChemBioChem 16(4):659–669. doi:10.1002/cbic.201402595
44. Jancso G, Domoki F, Santha P, Varga J, Fischer J, Orosz K, Penke B, Becskei A, Dux M, Toth L (1998) Beta-amyloid (1–42) peptide impairs blood-brain barrier function after intracarotid infusion in rats. Neurosci Lett 253(2):139–141
45. Edwin NJ, Hammer RP, McCarley RL, Russo PS (2010) Reversibility of beta-amyloid self-assembly: effects of pH and added salts assessed by fluorescence photobleaching recovery. Biomacromolecules 11(2):341–347. doi:10.1021/bm900833b
46. Reddy G, Straub JE, Thirumalai D (2009) Influence of preformed Asp23–Lys28 salt bridge on the conformational fluctuations of monomers and dimers of A beta peptides with implications for rates of fibril formation. J Phys Chem B 113(4):1162–1172. doi:10.1021/jp808914c
47. Uversky VN (2014) The triple power of D-3: protein intrinsic disorder in degenerative diseases. Front Biosci (Landmark) 19:181–258. doi:10.2741/4204